Data Analysis for Dynamics of Cooperative Bridge-Vehicle System Considering Pavement Roughness and Separation

Hui Chen, Wuyin Jin, and Jiamin Xuan

***Abstract*— A radial nonlinear multi-spring-damper tire (RNMST) model is proposed in this paper for dynamics behavior analysis of the cooperative bridge-vehicle (CBV) system by considering different road surface roughness and separation. First, both the finite element (FE) and force analysis of the RNMST model were analyzed and studied under different velocity and different class of road surfaces. The three types of tire models, nonlinear single-spring tire (NSST) model, nonlinear multi-spring tire model and RNMST model, were introduced as the vehicle tire devices for a quarter vehicle models into nonlinear cooperative bridge-vehicle system. The cooperative dynamics problem, alongside separation and the responses of road surface in terms of its uneven nature, is a typical dynamics problem with the nonlinearity of material which can be solved using the Newmark-β method. The comparison of the results demonstrated that the analysis of the dynamics of the cooperative bridge-vehicle system under the RNMST model and NMST model are generally similar. However, the radial nonlinear multi-spring-damper tire model is more accurate and closer to the stress state of the real tire model. Also, to further illustrate the comprehensive performance of the RNMST, the responses under different pavement excitations were analyzed by using the amplitude-frequency spectrum method. Finally, to research the influence dynamics of tire force on the CBV system, the horizontal component of tire force was analyzed. This is conducive to numerical research of the dynamic responses of both the bridge and the vehicle.**

***Index Terms*— Cooperative bridge-vehicle (CBV) system, horizontal component of tire force, pavement incentive, radial nonlinear multi-spring-damper tire (RNMST).**

I. Introduction

BRIDGES and vehicles as transportation infrastructures play a vital role in societal development. Also, the dynamics behaviors of cooperative bridge-vehicle (CBV) system have a huge impact on the vehicle performance, both the safety and service life of the bridge [1]–[4]. Introduce the coupling problem of the vehicle and the road into the field of vehicle and road design will influence the direction of future development, as proposed by Mamlouk in 1997 [5]. Dynamic behaviors of beam structures, such as bridges on highways, which are subject to moving loads have been researched for over a century since Stokes highlighted this problem [6]. In many engineering applications, the design of the highway, bridge, and tunnel are of great interests as well as how they incorporate these features, thus, a large number of papers related to this problem have been published to predict the dynamic responses of simple supporting structures under moving loads [7]–[13]. Dynamic vehicle loads have caused early road surface damages and has become a prominent problem in engineering. For instance, many of the asphalt-concrete pavement which are open to traffic in 2-3 years have different degrees of damage [14]. As a result, it is prudent to study the vehicle-road coupling dynamics and publish the finding accordingly.

CBV system has been researched for many years [15]–[17], in areas which focused on both the vehicle dynamics and road dynamics, as such there have been significant progress a number of scholars. In their researches, it was observed that, the vehicle can be used as a vibrator to study the vehicle dynamics and its properties. Many researchers have done a lot of researches on the cooperation system between the vehicle, the network, the grid, big data, blockchain and related content [18]–[20].Research on vibration characteristics of vehicle system based on deep learning theory and neural network theory is also a direction of vehicle dynamics research in recent years [21], [22].

The vehicle dynamics takes the road surface profile as the random excitation of the vehicle to study the maneuverability, comfort and safety performance of the vehicle system, while the road dynamics takes the vehicle as the moving load to study the responses and service life of the road. The parameters of tire pressure and road surface damage also have a great influence on vehicle dynamics response; when dynamic tire force is reduced by 15%, road surface damage is reduced by 5.2% [23]–[27]. Another application is to research indirect method of identifying bridge modal properties and its damages [28], [29]. Recently, it became increasingly popular because it is convenient, and it is “a step toward mobile infrastructure informatics in a large urban setting [30]”.

Bridge-vehicle model consists of vehicle suspension system, tire system, vehicle body and bridge model, which can be established by different methods [31]–[34]. In this aspect, the accuracy is highly related to the established model in the

Manuscript received December 22, 2020; revised March 13, 2021 and April 10, 2021; accepted April 17, 2021. This work was supported in part by the Key Research and Development Program of Gansu Province, China, under Grant 18YF1GA063. The Associate Editor for this article was S. H. Ahmed. *(Corresponding author: Wuyin Jin.)*

The authors are with the School of Mechanical and Electrical Engineering, Lanzhou University of Technology, Lanzhou 730050, China (e-mail: wuyinjin@hotmail.com; chenhui2896@163.com).

Digital Object Identifier 10.1109/TITS.2021.3075229

response to the dynamics analysis of the CBV model. So far, the single point contact (SPC) model, which is considered as the contact area between road and tire is assumed as a single point of contact, and is the most commonly used tire model for numerical research [35]. This is because the SPC model convenient for calculations and is therefore widely used in the vehicle model. The SPC performs better when low road roughness is applied to the vehicle, by ignoring the tire effective filtering for high frequency component in the road roughness, some researchers [36]–[39] found that the CBV structure in which the contact is treated as a point is not accurate if the road surface is exempted. As a result, the characteristics of the flexible elastic roller (FRC) tire model which affects the geometry of the tire filtering, and the elastic filtering replaces the SPC tire model is considered [40].

The study of the contact state between the tire and pavement surface is a very important topic. There are two common ways to simulate the tire contact state with pavement surface: one way is to consider the pavement and the tires separately, for each time, to think about the coupling of the pavement and the vehicle [41]–[43]. The other way is to consider the tire and the pavement surface as a coupling system, and carry out calculations and analysis by means of dynamics solution [44]–[46]. Zhu *et al.* proposed the NSST model by using the single point contact tire (SPC) model to analyze the coupling dynamic response process of the cooperative bridge-vehicle(CBV) system [47]. Zhang *et al.* proposed the NMST model to replace the NSST model by using it to study the dynamics response of the cooperative bridge-vehicle system [48]. The NMST model is more accurate than the NSST model, but it's still not accurate enough. The tire force consists of limited nonlinear multi-springs in parallel arrangement between spring and each other in the contact area, and each spring of which is arranged in parallel with the vertical displacements of the vehicle. Then there is a question: the deformation of springs model of the RNMST both in the edge location and the tire center of contact area will be approximately equal, and this state is without considering the road roughness, the vertical displacements of the vehicle and the effect of vertical deflection of bridge temporary, however, this approximation method is wrongly done in the actual tire operation environment.

RNMST model is proposed in this paper. By introducing the RNMST model into the CBV system which is a typical dynamics problem, we can then use a combination of Newmark-β methods to solve it, details available in section 2. The stochastic process of the road surface roughness and the white noise method as the excitation signal of cooperative vehicle-bridge system are explained in detail in section 3. In section 4, the proposed RNMST, NMST, and NSST are verified using numerical calculation. The comparison of NSST, NMST, and RNMST models show that the RNMST can predict more realistic dynamic responses than the NSST and NMST models. The results of numerical study are analyzed and discussed at the end of the paper. The radial nonlinear multi- spring-damper model is applied to a quarter vehicle model to study the coupling vibration characteristics of vehicle-bridge under the vehicle as moving load. Through comparative analysis, the proposed tire model has excellent dynamic response characteristics.

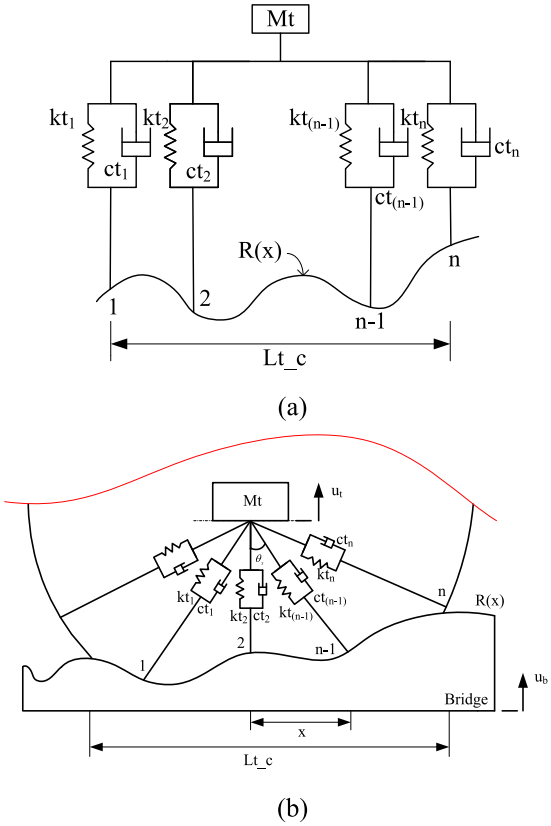

Fig. 1. Tire models (a) NMST model in [48] (b) Radial nonlinear multi-spring-damper tire (RNMST) model.

II. Dynamic Time Dependent Model of Cooperative Bridge-Vehicle (CBV) System

A. Radial Nonlinear Multi-Spring-Damper Tire (RNMST) Model

The NMST model was proposed by Zhang *et al.* in 2018 and Fig.1a is the structure diagram of the NMST model [48]. For this model, the spring and damping elements in the contact area are arranged in parallel to the vertical displacement of the vehicle.

Radial nonlinear multi-spring-damper tire (RNMST) model is proposed in this paper, with a schematic diagram shown in Fig.1b. The model consists of n independent and identical single nonlinear springs-damper elements in radial direction, and the structure of each single nonlinear spring-damper model is the same as the NSST model which was proposed in [47]. According to [37], [49], the radial mechanical performance of the tire of vehicle is modeled using continuous spring-damping elements, in which the spring-damper elements are uniformly distributed along the tire contour and tire width directions. To divide the X direction (as shown in Fig.2) of the contact area between tire and bridge into n equal small districts, the length of each small district Δn denotes the distance between the two adjacent single nonlinear springs-damper models in the horizontal direction X. The stiffness and damper

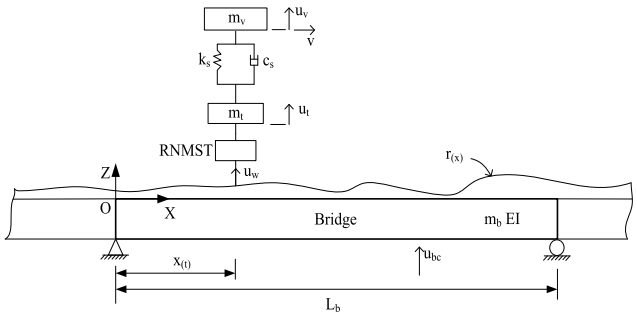

Fig. 2. Model of cooperative vehicle-bridge system.

coefficient of each spring-damper model under compression can be determined as follows:

$$k_{t,i} = k_t/n, \quad \mathrm{i} = 1, 2, \ldots, \mathrm{n} \tag{1a}$$

$$c_{t,i} = c_t/n, \quad \mathrm{i} = 1, 2, \ldots, \mathrm{n} \tag{1b}$$

In reference [50], the contact area of the bridge and tire is a single rectangle, and the length L_{c_t} is set as 25cm. It is assumed that the radial tire contact force is uniformly distributed along the width (axis of tire) direction of the tire.

The radial deformed length at the position x can be expressed as:

$$u_{d,x} = \frac{(u_t + u_{w,x} - lo(1 - \cos\theta_x))}{\cos\theta_x} \tag{2}$$

where, $u_{w,x}, u_t$ denote the vertical displacement at contact position x and vertical displacement of the tire center, lo is half the length of tire diameter minus tire hub diameter. The vertical displacement at position x can be written as:

$$u_{w,i} = u_{b,i} + r_i(x) \tag{3}$$

in which, $r_i(x)$ denotes the pavement profile roughness at the i-th single spring-damper model which will be covered in more detail in a later section of this paper, $u_{b,i}$ denotes the vertical displacement of bridge at contact position x.

The angle θ_x between the vertical displacement and the direction form the position x to the center (axis) of the tire can be expressed as:

$$\cos\theta_x = \frac{\sqrt{lo^2 - x^2}}{lo} \tag{4}$$

The nonlinear Hertz spring has been employed in this study, for each single spring-damper node, the stiffness can be expressed as:

$$k_{t,i} = \begin{cases} k_{t,i}(lo - l_{td,i})^{\frac{3}{2}}, & l_{td,i} < lo \\ 0, & l_{td,i} \geq lo \end{cases} \tag{5}$$

in which, $l_{td,i}$ denotes the deformed length of the nonlinear single spring-damper of the i-th node which defined as follow:

$$l_{td,i} = lo - u_{d,x} \tag{6}$$

B. Motion Equations of CVB Interaction System

As shown in Fig.2, the bridge model adopts the Euler beam with equal cross section, and the vehicle is modeled as an oscillator with 2 DOF. The sprung mass (vehicle body and vehicle suspension) and the tire are connected by a simple active suspension with stiffness k_s and damper c_s, the vehicle moves along the bridge at a constant velocity v with separation between the tire and the bridge. The vertical displacements u_v, u_t of both the spring mass m_v and the tire mass m_t are expressed in the matrix form:

$$\begin{bmatrix} m_v & 0 \\ 0 & m_t \end{bmatrix} \begin{pmatrix} \ddot{u}_v \\ \ddot{u}_t \end{pmatrix} + \begin{bmatrix} c_s & -c_s \\ -c_s & c_s + c_t \end{bmatrix} \begin{pmatrix} \dot{u}_v \\ \dot{u}_t \end{pmatrix} + \begin{bmatrix} k_s & -k_s \\ -k_s & k_s + k_t \end{bmatrix} \begin{pmatrix} u_v \\ u_t \end{pmatrix} = \begin{pmatrix} -m_v g \\ -m_t g + f_c(t) \end{pmatrix} \tag{7}$$

where, g is gravitational acceleration parameter and f_c denotes the interaction tire force at the tire contact area with the bridge pavement, and is expressed as:

$$f_c(t) = \sum_{i=1}^{n} f_{c,i}(t) \tag{8}$$

Eq. (7) can be reconstituted as matrix, in the form:

$$\mathbf{M}_v \ddot{\mathbf{u}}_v + \mathbf{C}_v \dot{\mathbf{u}}_v + \mathbf{K}_v \mathbf{u}_v = \mathbf{F}_v(t) \tag{9}$$

With reference to [15], [51], using the modal superposition method, the bridge motion equations can be expressed as:

$$\mathbf{M}_b \ddot{\mathbf{u}}_b + \mathbf{C}_b \dot{\mathbf{u}}_b + \mathbf{K}_b \mathbf{u}_b = \mathbf{F}_b(t) \tag{10}$$

in which, $\mathbf{M}_b, \mathbf{C}_b, \mathbf{K}_b$ are the mass, damper and stiffness matrices of the bridge, respectively, $\mathbf{u}_b$ is the modal coordinate generalized degree of freedom vector, $\mathbf{F}_b(t)$ is the dynamic load vector which interacting with the bridge, $\mathbf{u}_b(t)$ and $\mathbf{F}_b(t)$ are expressed as follows:

$$\mathbf{u}_b(t) = [\, u_{b1}(t) \quad u_{b2}(t) \quad \ldots \quad u_{bm}(t) \,]^{\mathbf{T}} \tag{11}$$

$$\mathbf{F}_b(t) = -\mathbf{F}_v(t) = -\mathbf{R}^{\mathrm{T}}(t)\, f_c(t) \tag{12}$$

in which, $\mathbf{R}(t)$ is the influence matrix and it can transform the non-node load of CBV system into equivalent load. The shape function vector of the bridge is given by:

$$\mathbf{\Phi}(t) = [\, \varphi_1(x) \quad \varphi_2(x) \quad \ldots \quad \varphi_m(x) \,] \tag{13}$$

where, $\varphi_1(x)\ \varphi_2(x)\ \ldots\ \varphi_m(x)$ denote the i-th mode shape function of the bridge, expressed as follows:

$$\varphi_i(x) = \sqrt{\frac{2}{m_b}} \sin(\frac{ipx}{L_b}), \quad i = 1, 2, \ldots, \mathrm{m} \tag{14}$$

where, m_b denotes the bridge mass, symbol "m" is the modal order of the bridge. The frequency of the bridge is:

$$\omega_i = \sqrt{(\frac{i\pi}{L_b})^4 \frac{EI}{m_b}}, \quad i = 1, 2, \ldots, \mathrm{m} \tag{15}$$

the bridge vertical displacement $u_{bc}(x, t)$ at the tire contact x, instantaneous time t is:

$$u_{bc}(x, t) = \sum_{i=1}^{m} \varphi_i(x) u_{bi}(t) = \mathbf{\Phi}(\boldsymbol{x}) \boldsymbol{u}_b \tag{16}$$

The cooperative force of bridge-vehicle at contact position $f_{c,i}$ in (8) can be expressed as:

$$f_{c,i} = \frac{c_t}{n}(\dot{u}_{dx,i}\cos\theta_x - \dot{u}_t) + \frac{k_t}{n}(u_{dx,i}\cos\theta_x - u_t) \quad (17)$$

Eq. (9) and (10) can be structured as follows:

$$\begin{aligned}
&\begin{bmatrix} m_v & 0 & 0 \\ 0 & m_t & 0 \\ 0 & 0 & \mathbf{M}_b \end{bmatrix}\begin{pmatrix} \ddot{u}_v \\ \ddot{u}_t \\ \ddot{\mathbf{u}}_b \end{pmatrix} \\
&\quad + \begin{bmatrix} c_s & -c_s & \mathbf{0} \\ -c_s & c_s + c_t & -\sum_{i=1}^{n} c_{t,i}\boldsymbol{\Phi}_\mathbf{i} \\ \mathbf{0} & \mathbf{0} & \mathbf{C_b} + \sum_{i=1}^{n} c_{t,i}\boldsymbol{\Phi}_\mathbf{i}^\mathbf{T}\boldsymbol{\Phi}_\mathbf{i} \end{bmatrix}\begin{pmatrix} \dot{u}_v \\ \dot{u}_t \\ \dot{\mathbf{u}}_b \end{pmatrix} \\
&\quad + \begin{bmatrix} k_s & -k_s & \mathbf{0} \\ -k_s & k_s + k_t & -\sum_{i=1}^{n} k_{t,i}\boldsymbol{\Phi}_\mathbf{i} \\ \mathbf{0} & \mathbf{0} & \mathbf{K}_b + \sum_{i=1}^{n} k_{t,i}\boldsymbol{\Phi}_\mathbf{i}^\mathbf{T}\boldsymbol{\Phi}_\mathbf{i} \end{bmatrix}\begin{pmatrix} u_v \\ u_t \\ \mathbf{u}_b \end{pmatrix} \\
&= \begin{pmatrix} -m_v g \\ -m_t g \\ \mathbf{0} \end{pmatrix} + \sum_{i=1}^{n}\begin{pmatrix} 0 \\ c_{t,i}(\dot{r}_i(x) - \sin\theta_x) \\ -\boldsymbol{\Phi}_\mathbf{i}^\mathbf{T} c_{t,i}(-\dot{r}_i(x) + \sin\theta_x) \end{pmatrix} \\
&\quad + \sum_{i=1}^{n}\begin{pmatrix} 0 \\ k_{t,i}(r_i(x) - lo + \cos\theta_x) \\ -\boldsymbol{\Phi}_\mathbf{i}^\mathbf{T} k_{t,i}(-r_i(x) + lo - \cos\theta_x) \end{pmatrix} \qquad (18)
\end{aligned}$$

in which, $\mathbf{M}_b, \mathbf{C}_b, \mathbf{K}_b$ are the mass, damper and stiffness matrices of the bridge which is defined as follows:

$$\mathbf{M}_b = diag(\frac{m_b}{2} \quad \frac{m_b}{2} \quad ... \quad \frac{m_b}{2}) \quad (19)$$

$$\mathbf{C}_b = m_b \cdot diag(\zeta_1\omega_1 \quad \zeta_2\omega_2 \quad ... \quad \zeta_m\omega_m) \quad (20)$$

$$\mathbf{K}_b = \frac{m_b}{2} \cdot diag(\omega_1^2 \quad \omega_2^2 \quad ... \quad \omega_m^2) \quad (21)$$

Eq. (18) can be rewritten in the general form:

$$\mathbf{M}\ddot{\mathbf{X}} + \mathbf{C}\dot{\mathbf{X}} + \mathbf{K}\mathbf{X} = \mathbf{F} \quad (22)$$

in which, **M,C,K** and **F** denotes mass, damper and stiffness matrices.

It's worth noting that to solve (22) that were solve a nonlinear process problem, because the shape function $\boldsymbol{\Phi}(t)$ is time-dependent. According to the method in [52], (22) can be solved.

The initial value of the velocity and displacement vector at $t = 0$ are assumed as follows:

$$\mathbf{X}_{t=0} = \dot{\mathbf{X}}_{t=0} = [0, 0, \ldots, 0]^\mathrm{T} \quad (23)$$

by solving the (12) and combining the (22) and (23), the acceleration vectors at time $t = 0$ can be derived from (12):

$$\ddot{\mathbf{X}}_{t=0} = \mathbf{M}^{-1}(\mathbf{F}_{t=0} - \mathbf{C}_{t=0}\dot{\mathbf{X}}_{t=0} - \mathbf{K}_{t=0}\dot{\mathbf{X}}_{t=0}) = \mathbf{M}^{-1}\mathbf{F}_{t=0} \quad (24)$$

it should be noted that mass matrix **M** is time-independent in this study. The dynamic responses of cooperative bridge-vehicle system at $t = t + \Delta t$ can be obtained by calculating following equation:

$$\mathbf{M}\ddot{\mathbf{X}}_{t+\Delta t} + \mathbf{C}_{t+\Delta t}\dot{\mathbf{X}}_{t+\Delta t} + \mathbf{K}_{t+\Delta t}\mathbf{X}_{t+\Delta t} = \mathbf{F}_{t+\Delta t} \quad (25)$$

in which, $\mathbf{C}_{t+\Delta t}, \mathbf{K}_{t+\Delta t}, \mathbf{F}_{t+\Delta t}$ are damper, stiffness matrices and force vector at time of $t = t + \Delta t$, which are velocity and displacement dependent.

By using Newmark-β method, the initial displacement and velocity vectors at $t = t + \Delta t$ is given below as:

$$\dot{\mathbf{X}}_{t+\Delta t} = \dot{\mathbf{X}}_t + [(1-\beta)\ddot{\mathbf{X}}_t + \beta\ddot{\mathbf{X}}_{1+\Delta t}]\Delta t \quad (26)$$

$$\mathbf{X}_{t+\Delta t} = \mathbf{X}_t + \dot{\mathbf{X}}_t\Delta t + [(\frac{1}{2} - \gamma)\ddot{\mathbf{X}}_t + \gamma\ddot{\mathbf{X}}_{t+\Delta t}]\Delta t^2 \quad (27)$$

$\dot{\mathbf{X}}_{t+\Delta t}, \ddot{\mathbf{X}}_{t+\Delta t}$ can be obtained by calculating the (26-27):

$$\ddot{\mathbf{X}}_{t+\Delta t} = a_0(\mathbf{X}_{t+\Delta t} - \mathbf{X}_t) - a_2\dot{\mathbf{X}}_t - a_3\ddot{\mathbf{X}}_t \quad (28)$$

$$\dot{\mathbf{X}}_{t+\Delta t} = a_1(\mathbf{X}_{t+\Delta t} - \mathbf{X}_t) - a_4\dot{\mathbf{X}}_t - a_5\ddot{\mathbf{X}}_t \quad (29)$$

where, $a_0, a_1, a_2, a_3, a_4, a_5$ denote integral coefficients which have been given in the A1 of Appendix A.

Equivalent stiffness matrix can be defined as:

$$\bar{\mathbf{K}} = \mathbf{K} + a_0\mathbf{M} + a_1\mathbf{C} \quad (30)$$

The instantaneous force vector at time step $t = t + \Delta t$ is calculated as follow:

$$\begin{aligned}
\bar{\mathbf{F}}_{t+\Delta t} = \mathbf{F}_{t+\Delta t} &+ \mathbf{M}(a_0\mathbf{X}_t + a_2\dot{\mathbf{X}}_t + a_3\ddot{\mathbf{X}}_t) \\
&+ \mathbf{C}(a_1\mathbf{X}_t + a_4\dot{\mathbf{X}}_t + a_5\ddot{\mathbf{X}}_t) \quad (31)
\end{aligned}$$

The displacement, velocity, and acceleration vectors at $t + \Delta t$ can be calculated by time step:

$$\mathbf{X}_{t+\Delta t} = \bar{\mathbf{K}}^{-1}\bar{\mathbf{F}}_{t+\Delta t} \quad (32)$$

$$\ddot{\mathbf{X}}_{t+\Delta t} = a_0(\mathbf{X}_{t+\Delta t} - \mathbf{X}_t) - a_2\dot{\mathbf{X}}_t - a_3\ddot{\mathbf{X}}_t \quad (33)$$

$$\dot{\mathbf{X}}_{t+\Delta t} = a_7\ddot{\mathbf{X}}_{t+\Delta t} + \dot{\mathbf{X}}_{tt} + a_6\ddot{\mathbf{X}}_t \quad (34)$$

where, a_6, a_7 denote integral coefficients which have been given in the A2 of Appendix A.

III. Identification Algorithm of Road Surface Roughness

A. Pavement Type 1

There are many approaches to mimic pavement stimulation. One is the method of power spectrum density spectrum of standard pavement [53]. The distribution of unilateral power spectral density is:

$$G_{(n,i)} = G_{(n_0)}(\frac{n_i}{n_0})^{-2} \quad (35)$$

in which, $G_{(n_0)}$ is the unilateral power spectral density of the reference spatial frequency n_0, n_i is the i-th spatial frequency component. Parameters of $n_0 = 0.1\mathrm{m}^{-1}$, $G_{(n_0)} = 16 \times 10^{-6}\mathrm{m}^3$/cycle are used to simulate grade -A pavement excitation in this study.

The pavement excitation can be expressed as follows:

$$r(x) = \sum_{i=1}^{N}\sqrt{2G(\mathrm{n}_i)\Delta h}\cdot\cos(2\pi n_i x + \theta_i) \quad (36)$$

where, x is the distance along the pavement, $n_i = i \cdot \Delta h$ denotes the i-th spatial frequency component, and θ_i denotes

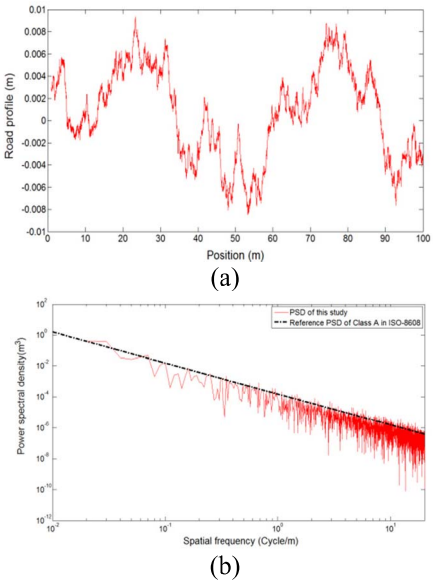

Fig. 3. Pavement surface roughness profile 1 (Grade-A) (a) Pavement profile (b) unilateral PSD.

a set of random phase angle which follows uniform distributed form $[0, 2\pi]$,divide the frequency range into N equal intervals, and $N = L/(2\Delta x)$, Δx is the spatial increment which set as 0.001m (1mm) in this study [54], [55]. Δh is the frequency spacing which can be determined as follow:

$$\Delta h = \frac{(n_{\max} - n_{\min})}{N} \tag{37}$$

in which, $n_{\max}, n_{\min}$ denote the upper and lower spatial frequency limits, respectively. With the ISO-8608 [53], the spatial frequency $n \in [0.01, 20]m^{-1}$ in this study. Fig.3 shows the Pavement type 1(abbreviate as PT1), Grade-A, the bridge length $L_b = 25$m and its unilateral power spectrum density.

B. Pavement Type 2

The second method to generated pavement profile considered is composed of first-order low-pass filter white noise signal in this study. For reference and comparison with pavement type 1, the parameter was set to 0.005 for Grade-A pavement using the normalization method.

Fig.4 shows the pavement surface roughness type 2 (abbreviate as PT2), Grade-A, $L_b = 25$m and its unilateral power spectrum density.

Fig. 4c is the structure diagram of the Band-limited white noise signal generated in *Matlab* software. The signal generator composed of the white noise signal and a low-pass filter, and the transfer function of the filter can be expressed as:

$$G(s) = \frac{a}{s + a} \tag{38}$$

It can be clearly seen that the pavement roughness surface and its unilateral PSD generated by this method is consistent with the noise measured method from [53] in Fig.4.

Fig.3 and Fig.4 show the two kinds of pavement roughness generated by a zero-mean stationary Gaussian random

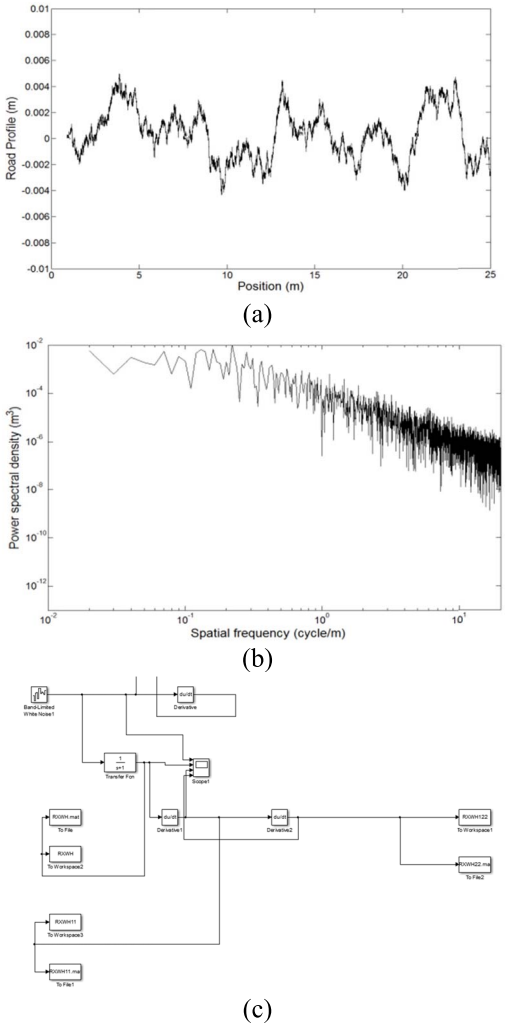

Fig. 4. Pavement surface roughness type 2 (Grade-A) (a) Pavement profile (b) unilateral power spectrum density (c) Structure diagram of simulation.

process(Pavement type 1,PT1) and a set of first-order low -pass filters with a white noise input(Pavement type 2,PT2). The pavement roughness of PT1 is distributed between -0.01m and 0.01m, whereas, the PT2 is distributed between -0.004m and 0.005m, the displacement power spectral density of PT1 is $(10^{-10},10^{0})$ m^3, and that of PT2 is $(10^{-8},10^{-2})$m3. It can be clearly seen from Fig.3 and Fig.4 that PT2 is obviously smoother than PT1.

IV. Numerical Examples

The vehicle-bridge models as shown in Fig.2 and the parameters of which are referenced in the Appendix B, illustrates how to validate the response of the RNMST model in cooperative bridge-vehicle (CBV) system and compare it with both NSST model and NMST model. Two different types of pavements, pavement roughness type 1 generated by unilateral PSD approach and pavement roughness type 2 generated by series of first-order low-pass filter with white noise, and different standards of pavements grade and velocity of vehicle were adopted: Grade-A, for pavement type 1 and Grade-A, for pavement type 2 were adopted.

TABLE I

MAXIMUM AND MINIMUM VALUES OF DISPLACEMENT, VELOCITY AND ACCELERATION OF VEHICLE, TIRE AND BRIDGE UNDER DIFFERENT ROAD PROFILE

Pavement type	**Pavement type 1, 5m/s , Grade -A**						**Pavement type 2, 20m/s ,Grade-A**					
Tire model	NSST		NMST		RNMST		NSST		NMST		RNMST	
Value	Min	Max	Min	Max	Min	Max	Min	Max	Min	Max	Min	Max
Displacement of vehicle (m)	-0.0773	0	-0.0767	0	-0.0716	0	-0.0708	0	-0.0700	0	-0.0653	0
Displacement of tire (m/s)	-0.0719	0	-0.0715	0	-0.0667	0	-0.0654	4.2116×10^{-4}	-0.0648	0	-0.0605	0
Velocity of vehicle (m/s)	-0.5089	0.4249	-0.0616	0.0528	-0.0410	0.0352	-0.2455	0.2137	-0.0295	0.0270	-0.0198	0.0193
Velocity of tire(m/s)	-0.3920	0.2378	-0.0411	0.0286	-0.0305	0.0196	-0.1866	0.1168	-0.0197	0.0188	-0.0182	0.0180
Acceleration of vehicle (m/s^2)	-12.0831	12.6749	-1.5108	1.6159	-1.0013	1.1171	-9.8000	6.2667	-0.7655	0.8335	-0.5268	0.5673
Acceleration of tire (m/s^2)	-12.4193	22.1495	-0.8317	1.2726	-0.5679	0.8853	-12.1970	11.0494	-0.6547	0.5457	-0.4618	0.3916
Displacement of bridge (m)	-0.0593	$34465\times10^{-1}_{0}$	-0.0589	0	-0.0550	0	-0.0601	5.6014×10^{-9}	-0.0596	9.3465×10^{-10}	-0.0556	8.3574×10^{-10}
Velocity of bridge (m/s)	-0.0317	0.0339	-0.0180	0.0173	-0.0171	0.0164	-0.0400	0.0365	-0.0174	0.0176	-0.0163	0.0165
Acceleration of bridge (m/s^2)	-1.1173	1.0779	-0.2259	0.2457	-0.2003	0.2249	-2.5878	2.9443	-0.2948	0.2271	-0.2636	0.2073

In theory, the vibration analysis of a bridge, or the result of simulation calculation, the bridge vibration modes order has direct impact on the precision of calculation, thus, the higher the order number, the higher the precision. In this study, we adopted 5 order vibration modes of the bridge.

A. Responses of Pavement type1

Displacement, velocity and acceleration responses of vehicle and tire are shown in Fig.5. During the process of the vehicle moving on the bridge, and due to the deformation of the bridge, the vehicle displacement presents a symmetrical distribution of the midpoint position of bridge in Fig.5(a). However, the maximum displacement of the vehicle for NSST, NMST and RNMST model are -0.0773m, -0.0767m and -0.0716m, and not in the middle position of the bridge, but in the later position of the middle bridge position in Fig. 5a,b.The vehicle's velocity response curve enters the steady-state response process after the initial transient response of less than 0.1 seconds, and the velocity is between -0.05m/s and 0.05m/s. The maximum value of vehicle velocity are 0.4249m/s, 0.0528m/s and 0.0352m/s and the maximum value of tire velocity are 0.2378m/s, 0.0286m/s and 0.0196m/s by adopting different tire models of NSST, NMST and RNMST model in Fig.5c,d, respectively. The maximum value of vehicle acceleration are 12.6749m/s^2, 1.6159m/s^2 and 1.1171m/s^2 and the maximum value of tire velocity are 22.1496m/s^2, 1.2726m/s^2 and 0.8853m/s^2 by adopting different tire models of NSST, NMST and RNMST model, and the acceleration is between -1m/s^2 and 1m/s^2 (Do not count towards the transient response of less than 0.1 seconds)in Fig.5e,f.

By analyzing the acceleration, the velocity and displacement responses of vehicle and tire, it can be found that the RNMST model performs well than both NSST and NMST model, especially in response of velocity and acceleration.

Fig. 6a, Fig.6c and Fig.6e show the response of the bridge displacement, velocity and acceleration, respectively, and their responses in partial enlarged view. The displacement response of the bridge, similar to the response curve of vehicle displacement, is also symmetric about the central position (length direction of X) of the bridge. Therefore, the overall characteristics of the response curve of the bridge's velocity and acceleration are as follows: the two sides are relatively small while the middle position is relatively large. The values of the maximum and minimum responses of the bridge under different road profile types are shown in Table I. It can be clearly seen from the Fig.6b, Fig.6d and Fig.6f that a great difference on velocity and acceleration responses for different tire types, especially, the greatest impact on acceleration response: the ratio between the maximum acceleration response value 1.0779 m/s^2 and the maximum acceleration response value 0.2249 m/s^2 for NSST and RNMST model is 4.7927 times(dimensionless).

B. Responses of Pavement Type 2

Fig.7 shows the displacement, velocity and acceleration responses of vehicle and tire. The vehicle response for pavement profile 2 is generally similar to the vehicle response curve under pavement profile 1. The main difference is the magnitude of the amplitude, because pavement profile 2 is generated by the white noise signal method and the vehicle velocity $v_2 = 20$m/s, which is a little smoother in amplitude than the pavement profile 1. It clearly shows that the responses of displacement, velocity and acceleration are relatively wide in amplitude while pavement profile 2 was adopted by comparing both pavement profile 1 and pavement profile 2 as input excitation of cooperative vehicle-bridge system. The response values are illustrated in TableI.

It clearly seen in Fig.8 that the displacement response of the bridge is generally negative (in the opposite direction of Z axis), because the bridge deformation caused by its own weight and the movement of vehicle is consistent with the actual situation. At the same time, the response curve presents an approximately symmetrical view on the middle position of the bridge (direction X). It can be seen more clearly from the local magnified image Fig.8b that the displacement response distribution are completely different by adopting different tire models, the displacement response value of the bridge is minimal when the RNMST model is adopted, while the displacement response value of the bridge is maximized when the NSST model is adopted. For the specific displacement response data refer to Table I. As shown in Fig. 8a and

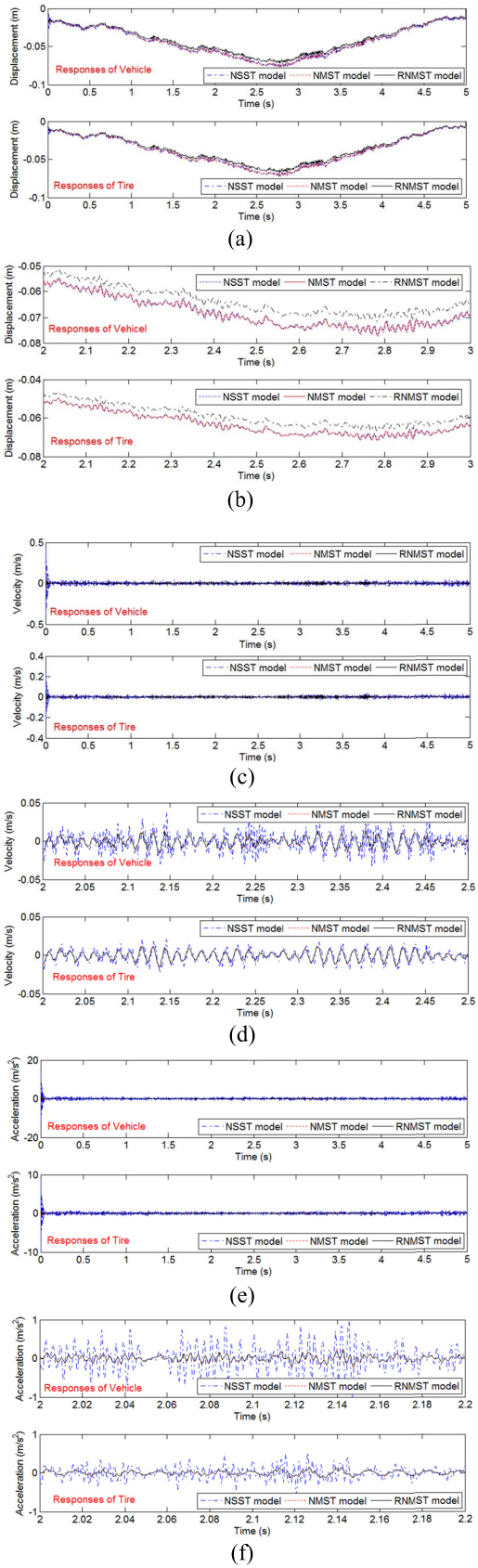

Fig. 5. Dynamics responses of vehicle and tire of pavement type 1, Grade-A, v_1 = 5m/s (a) displacement (b) displacement in partial enlarged view (c) velocity (d) velocity in partial enlarged view (e) acceleration (f)acceleration in partial enlarged view.

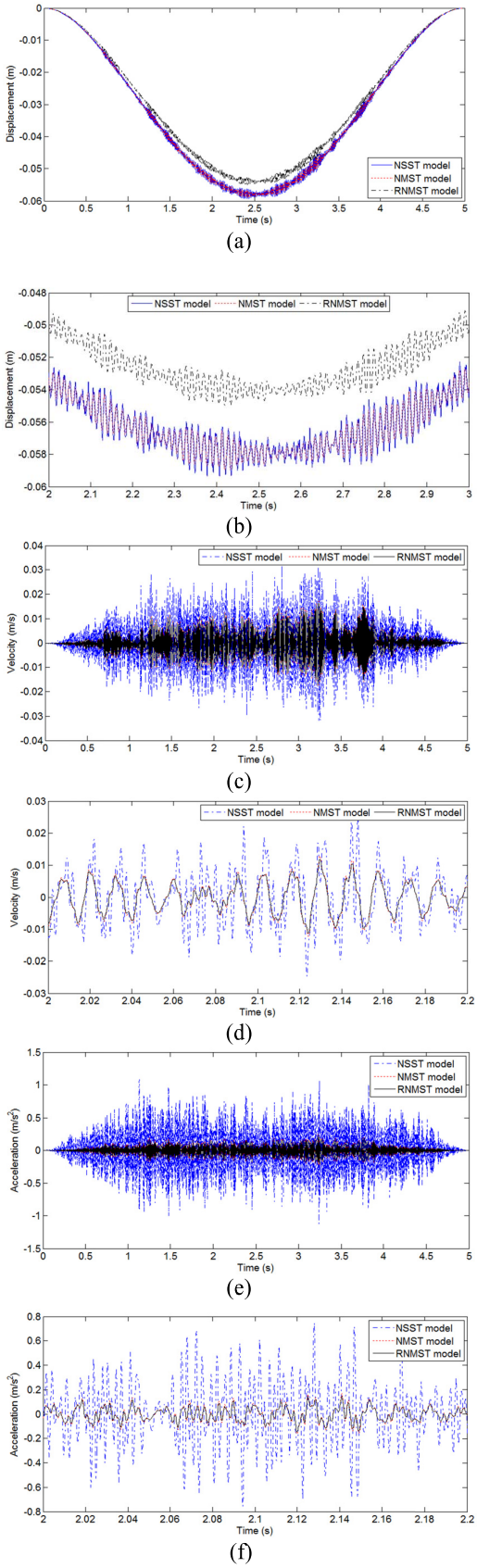

Fig. 6. Dynamic response of bridge for pavement type 2 of Grade-A, $v_2 = 20$m/s (a) displacement (b) displacement in partial enlarged view (c)velocity (d) velocity in partial enlarged view (e) acceleration (f) acceleration in partial enlarged view.

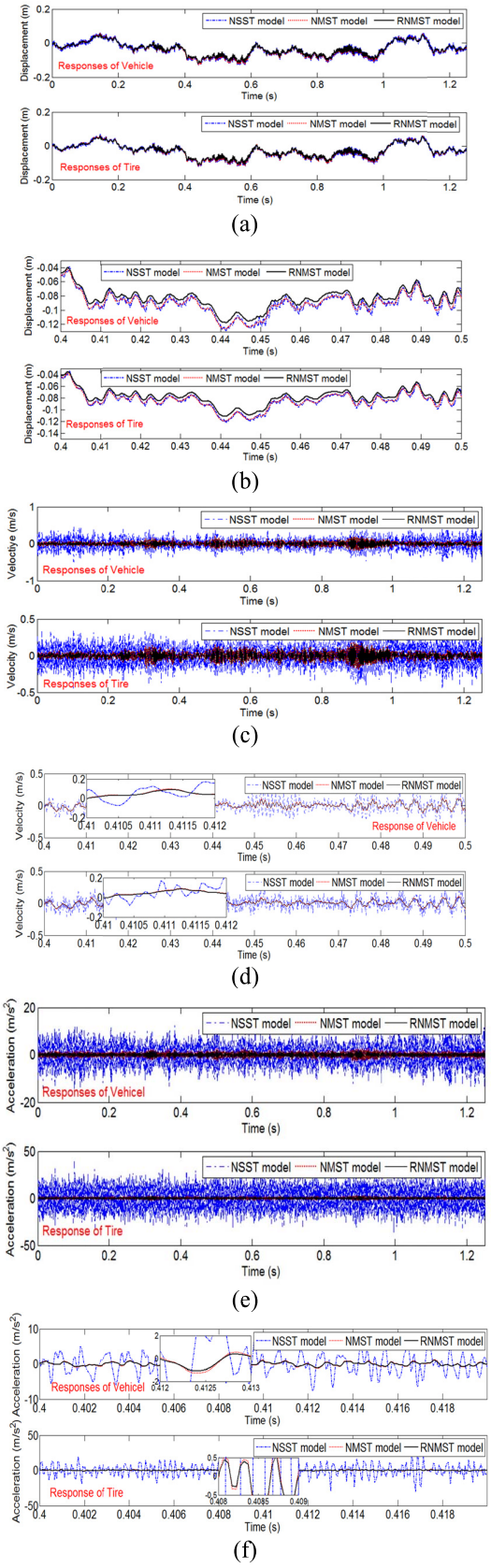

Fig. 7. Dynamic responses of vehicle and Tire for pavement type 2 of Grade-A, $v_2 = 20$m/s (a) displacement (b) displacement in partial enlarged view (c) velocity (d) velocity in partial enlarged view (e) acceleration (f) acceleration in partial enlarged view.

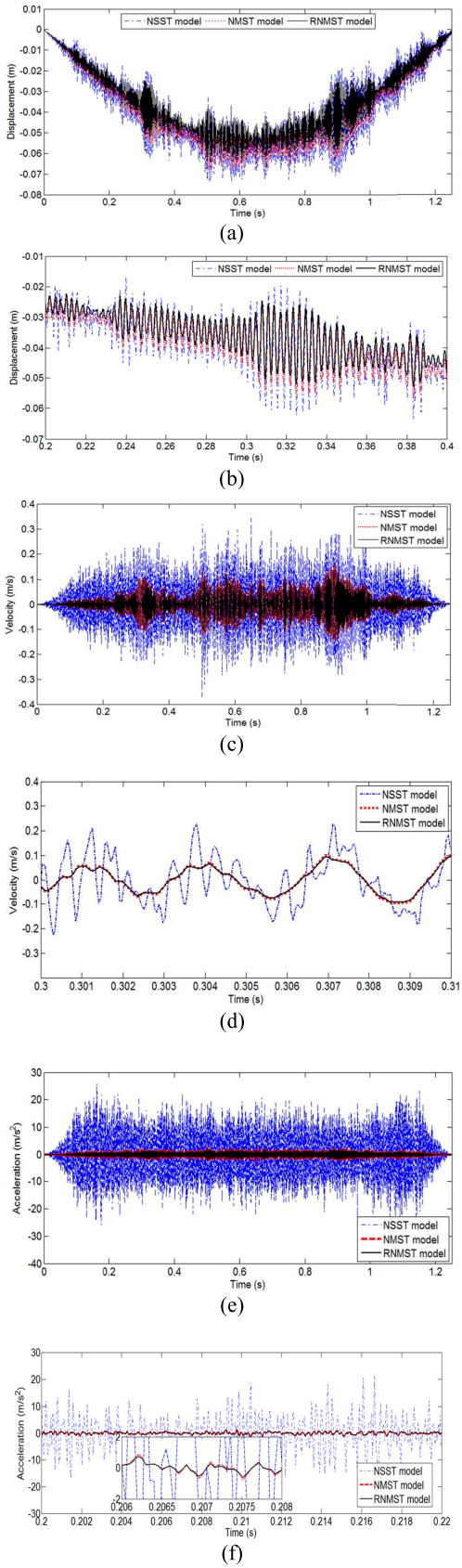

Fig. 8. Dynamics responses of the bridge, pavement 2 of Grade-A, $v_2 = 20$m/s(a) displacement of bridge (b) displacement of bridge in partial enlarged view (c) velocity (d) velocity in partial enlarged view (e)acceleration (f) acceleration in partial enlarged view.

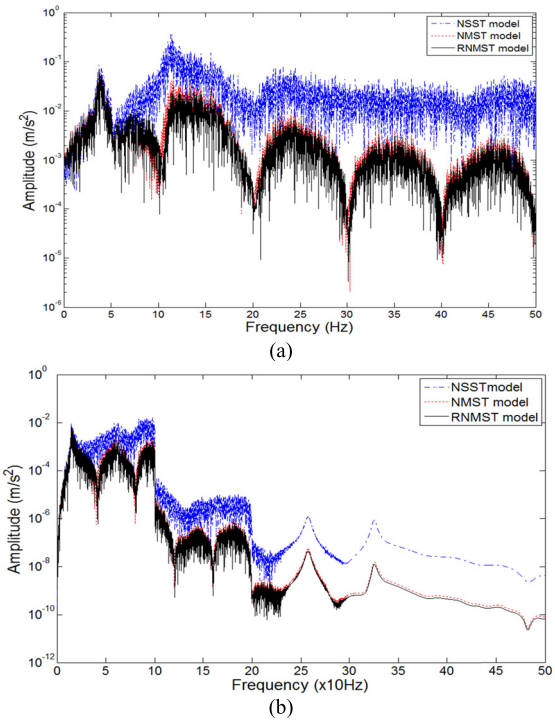

Fig. 9. Amplitude spectrum of the accelerations of (a) vehicle (b) birdge, pavement type 1, $v_1 = 5$m/s, Grade-A.

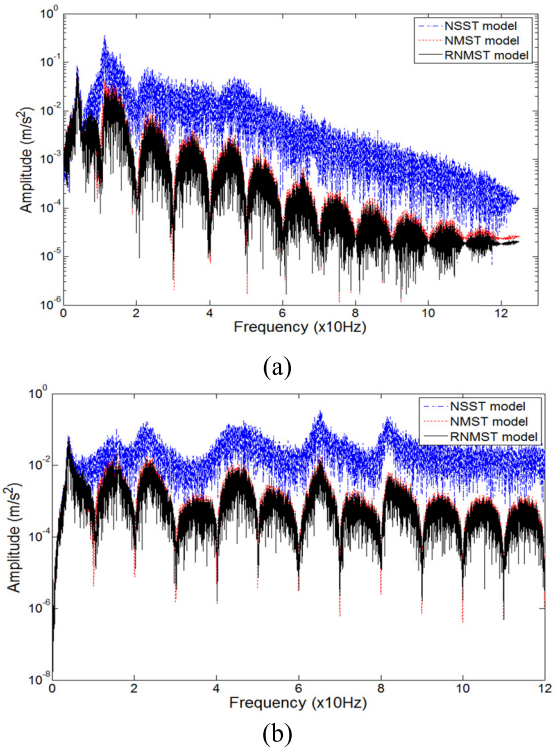

Fig. 10. Amplitude spectrum of the accelerations of (a) vehicle and (b) bridge, pavement type 2, $v_2 = 20$m/s, Grade-A.

Fig. 8b, the process of separation and re-contact between tire and pavement is quite obvious when the vehicle is running on the bridge: the tire is subjected to the interaction force of body gravity and pavement in Fig.11b, separation occurred between the tire and the pavement (bridge) surface in the time interval of 0.2 to 0.4 seconds. As can be clearly seen from Fig.8b, separation occurred between the tire and the pavement surface in the time interval of 0.34 to 0.38 seconds, so the displacement of the bridge was significantly reduced.

Fig.8c and Fig.8e describe the response of the bridge's velocity and acceleration. It can be seen intuitively that the velocity image and acceleration image present a symmetric image with the bridge as the axis of symmetry. The response of different tire models is greatly different, especially in the acceleration response image. By analyzing the data in Table I, it can be seen that the ratio of the maximum acceleration value 2.9443m/s^2 when NSST model is adopted to that 0.2073m/s^2 when RNMST tire model is adopted is 14.20308 (dimensionless), and it can be seen more clearly in Fig.8d and Fig. 8f.

C. Amplitude Spectrum of Vehicle and Bridge in Frequency Domain

In order to further illustrate the effect of RNMST model on reducing the amplitude of high-frequency components of dynamic response, the acceleration spectra of vehicles and bridge for pavement contour type 1 and pavement contour type 2 at different velocity levels are given in Fig.9 and Fig.10. It can be observed in Fig.9 that when the velocity is 5 m/s, generally, six peaks correspond to the 1st, 3rd, 5th, 7th and 9th frequencies of the bridge and the vehicle, which represents the natural frequency of the vehicle and the bridge. The odd frequency point can be observed because the midspan is the modal point of the even order modes. Due to the movement of the vehicle on the bridge, the half drive frequency should also be shown in the image theoretically, however, the half driving frequency cannot be observed in the Fig.9 and Fig.10, this is because of the acceleration amplitude spectrum drawn at the velocity of 5m/s. According to the analysis in [31],the amplitude of the half driving frequency in the spectrum of displacement is larger than that in the spectrum of the acceleration, and moreover, it's larger while the velocity is higher.

In the amplitude spectrum, the maximum value is 1.1171m/s^2 and 0.2249m/s^2, peaks that appear at the point with natural frequency of both vehicle and bridge. It can be seen from the amplitude spectrum, the RNMST model while maintaining the low frequency components that the amplitude of high frequency components reduces significantly. Also, from the diagrams, for different pavement types, the RNMST model and NMST model, the high frequency part of the component is approximately the same. In the actual cases, due to the movement of the vehicles on the bridge, the vibration in the bridge, need a certain speed, but for the low velocity of vehicle, high frequency vibration of bridge is almost faint.

As shown in Fig.10 for the amplitude spectrum of the acceleration response of the vehicle and the bridge under the pavement type 2. In addition to the driving frequency in Fig.10a, it can identify bridge fundamental frequency and the vehicle.

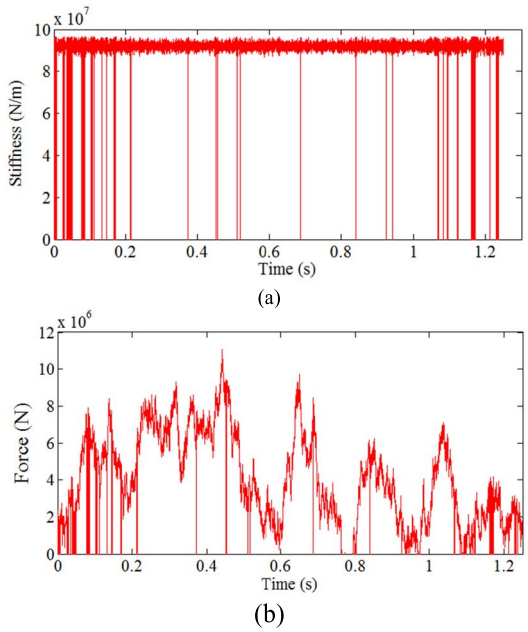

Fig. 11. The stiffness and the interaction force of tire, pavement type 2, Grade-A, $v_2 = 20$m/s (a) The spring stiffness of tire model (b) interaction fore of tire.

Amplitude spectrum of the vehicle and the bridge for different grades of road and velocity excitation are shown in Fig. 9 and Fig.10, it shows that RNMST model displays outstanding characteristics in frequency response, especially in the high-frequency part.

D. Stiffness of Nonlinear Tire With Separation

When the deformed length of one nonlinear spring model $u_{d,x} = 0$m, the state of separation between the tire and the pavement is considered, with the tire force at contact position $f_{c.i} = 0$N.

Fig. 11 shows the change of both the spring stiffness in the tire model and the interaction tire force from the body and the road surface when the vehicle runs over a bridge with a length of 25m at a constant velocity of 20m/s. When there is no separation state in the process of driving, the stiffness of the tire is probably distributed around in $\left(8.5 \times 10^7, 9.5 \times 10^7\right)$ N/m, and the interaction tire force is also randomly distributed in $\left(-0.65 \times 10^7, 0.65 \times 10^7\right)$ N.

It can be observed from the Fig.11 that the spring stiffness of tire model and interaction tire force changed to zero when the separation occurred.

E. The Horizontal (Direction X) Component of the Tire Force

The tire model in the contact area is considered to be composed of a finite number of nonlinear spring-damper models of RNMST model. Therefore, the tire force generated by the compression of each spring-damper model, there exists both horizontal (direction X) and vertical (direction Y) components, and this force exerts an influence on the vehicle. It can be intuitively observed from the Fig.12 that in the contact area between the tire and the pavement, the horizontal (direction X)

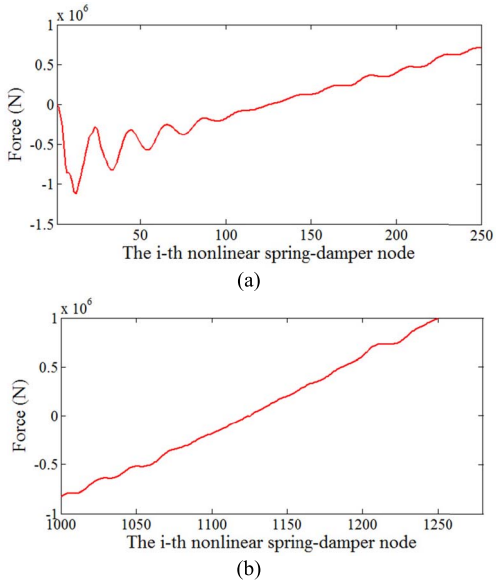

Fig. 12. The horizontal component of the tire force.

component of the tire force is not completely symmetrical to the middle position of the spring-damper node of the RNMST model, it is noteworthy that the Fig.12 only describes the horizontal component of the tire force. Theoretically, the right side of the tire contact area is positive, and the left side is negative, and the direction of the force can also be defined according to the specific application.

In the process of simulation, the system always needs to collect the force of K_N nodes which can be expressed as follow:

$$K_N = \frac{L_b}{\Delta h} \tag{39}$$

where, L_b denotes the length of the bridge, and which is set as 25m. Δh is the sample interval which is set as 0.01m in this paper.

The force of the i-th nonlinear spring-damper at an instantaneous moment is shown in Fig.12. Horizontal axis denotes the node of the tire contact area which is divided into many small intervals, each interval denotes a spring-damper model. Fig.12a and Fig.12b represent the forces on 250 nodes in the contact region. It is obvious from the Fig.12 that there is a significant change in the image at the center of the contact area (the 125^{th} node in Fig.12a and the 1125^{th} node in the Fig.12b).

V. Discussions

A. RNMST and NMST model have different properties, they do not only have the horizontal components of tire force but also have vertical components. The horizontal components of tire force can affect the ride comfort and overall performance of the vehicle, but the impact is slight.

TABLE II

MAJOR NOMENCLATURE AND PARAMETERS OF COOPERATIVE BRIDGE-VEHICLE SYSTEM USED IN THIS STUDY[1]

Symbols	Description	Unit	Value
u_v, u_t	Vertical displacement of the vehicle and tire	m	-
$\dot{u}_v, \dot{u}_t$	Vertical velocity of the vehicle and tire	m/s	-
$\ddot{u}_v, \ddot{u}_t$	Vertical acceleration of the vehicle and tire	m/s^2	--
u_w	Vertical displacement at the bridge contact position	m	-
$\mathbf{u_b}$	Generalized DOF vector in modal coordinate of bridge	m	-
u_{bc}	Vertical displacement of bridge	m	-
$\ddot{\mathbf{u}}_\mathbf{b}, \dot{\mathbf{u}}_\mathbf{b}$	Vertical acceleration and velocity of generalized DOF vector in modal coordinate of bridge	m/s^2, m/s	-
$\ddot{\mathbf{X}}, \dot{\mathbf{X}}, \mathbf{X}$	Acceleration, velocity and displacement vectors	m/s^2, m/s, m	-
$\mathbf{R(t)}$	Influence matrix	-	-
$\mathbf{\Phi(t)}$	Modal shape function of bridge	-	-
φ_i	Modal shape function of the *i*-th order of bridge	-	-
$\mathbf{M_v}, \mathbf{C_v}, \mathbf{K_v}$	Mass, damping and stiffness matrices of the vehicle	-	-
$\mathbf{M}_b, \mathbf{C}_b, \mathbf{K}_b$	Mass, damping and stiffness matrices of the bridge	-	-
$\mathbf{F_b(t)}, \mathbf{F_v(t)}$	Dynamic load vector of the bridge and vehicle	N	-
$f_{c,i}$	Interaction force of vehicle-bridge at contact point	N	-
k_s, k_t	Stiffness of the suspension and tire	N/m	9.14x10^7,1.08x10^9
c_s, c_t	Damping of the suspension and tire	Kg/s	5.24x10^5,2.9 x10^3
ω	Frequency of the bridge	rad	-
u_{dx}	Radial deformed length at the contact position	m	-
$l_{td,i}$	Deformed length of the nonlinear spring-damping of *i*-th node	m	-
θ_x	Angle between the vertical displacement and the direction form the contact position to the centerline (axis) of the tire	rad	-
r(x)	Road surface roughness profile	m	-
m_b	Mass of bridge	Kg	$A \cdot L_b \cdot \rho$
m_v	Mass of vehicle	Kg	4.8x10^4
M_t	Mass of tire	Kg	1.2x10^4
lo	Original length of tire (no stress status)	m	0.2
m	The modal order of the bridge	-	5
L_b	Length of the bridge	m	25
E	Young's modulus of bridge	GPa	27.5
I	Moment of inertia of bridge	m^4	0.12
A	Cross-sectional area	m^2	2
ρ	Density of bridge	Kg/m^3	2400
β	Parameter of Newmark- β	-	0.5
γ	Parameter of Newmark- β	-	0.25
n_0	Reference spatial frequency	Hz	0.1
ξ	Modal-damping ratio	-	0.02
$G(n_0)$	Unilateral PSD for the reference spatial frequency	m^3/cycle	16x10^{-6}

B. Both the RNMST model proposed in this paper and the NMST model in [48] is considered. The tire mass is distributed in the center axis of the tire, which is unreasonable in the actual situation, because the mass distributed at the edge the tire generates a great force with increase in vehicle velocity.

C. The dynamic characteristics of the cooperative bridge-vehicle system is studied only by using the vehicle as the vibration exciter, but the natural environment influence on the bridge, such as strong wind and rainstorm, are not taken into account. This has an impact on the accuracy of simulation.

D. The influence of rain, especially snow, on the tire-bridge contact surface was not considered. This also has an impact on the simulation results.

E. The radial nonlinear multi-spring damper tire model was introduced into the 1/4 vehicle system to study the dynamics characteristics under different external excitation, the actual vehicle has pitch, roll and yaw angular displacements, and these influences will be studied in future work.

[1]The parameters value of both vehicle and bridge are refer to the [21]

VI. CONCLUSION

In this paper, an improvement was made on the NMST model, the RNMST model is proposed and its dynamic response in relation to acceleration was studied, by introducing the velocity and the displacement into the cooperative bridge-vehicle system. The stiffness and damping of vehicle are time-dependent, so the length of each spring-damper model of the RNMST model must be calculated for each step, and then compare the output with initial deformation to determine which branch of stiffness should be used. Infinite iterations are adopted in the calculation, especially in the nonlinear system in this calculation process. For those reasons, the Newmark-β method is adopted in this paper.

After the simulation calculation, it was found that the RNMST model confirmed more excellent characteristics of the acceleration, velocity and displacement response than both the NSST and NMST model. It is clear that the comprehensive performance of RNMST model has advantages over the NMST and NSST model from the response analysis by comparing the amplitude spectrum with the pavement type 1, Grade-A, vehicle velocity of 5m/s and pavement type 2, Grade-A, vehicle velocity of 20m/s are used..

The RNMST model should be used to replace the NMST model not only in the cooperative vehicle-bridge system, but also in the process of vehicle dynamic response analysis system based on the research and analysis in this article. Research on the horizontal component of tire force (direction X) in this paper can be introduced into the whole vehicle model because of the overall stability of vehicle influenced by interaction tire force. In addition, considering the application of tire pressure in vehicle dynamics, the conclusions of this paper can also be used to directly measure modal parameters and define bridge strain and deflection.

DECLARATION OF COMPETING INTEREST

The author stated: no interest disputes between partners such as questions about the content of this article.

APPENDIX A
INTEGRAL COEFFICIENTS

The integral coefficients are defined as follows:

$$\alpha_0 = \frac{1}{\gamma\,\Delta t^2},\quad \alpha_1 = \frac{\beta}{\gamma\,\Delta t},\ \alpha_2 = \frac{1}{\gamma\,\Delta t},$$
$$\alpha_3 = \frac{1}{2\gamma} - 1,\quad \alpha_4 = \frac{\beta}{\gamma} - 1,\ \alpha_5 = \frac{\Delta t}{2}\left(\frac{\beta}{\gamma} - 2\right) \quad \text{(A1)}$$
$$\alpha_6 = \Delta t(1-\beta),\quad \alpha_7 = \Delta t\beta \quad \text{(A2)}$$

APPENDIX B
NOMENCLATURE AND PARAMETERS

See Table II.

APPENDIX C
SUPPLEMENTARY DATA

All the data involved are provided in the article.

REFERENCES

[1] H. Wang, J.-X. Mao, and B. F. Spencer, "A monitoring-based approach for evaluating dynamic responses of riding vehicle on long-span bridge under strong winds," *Eng. Struct.*, vol. 189, pp. 35–47, Jun. 2019.

[2] S. Borjigin, C.-W. Kim, K.-C. Chang, and K. Sugiura, "Nonlinear dynamic response analysis of vehicle–bridge interactive system under strong Earthquakes," *Eng. Struct.*, vol. 176, pp. 500–521, Dec. 2018.

[3] L. Hu *et al.*, "A multiobjective optimization approach for COLREGs-compliant path planning of autonomous surface vehicles verified on networked bridge simulators," *IEEE Trans. Intell. Transp. Syst.*, vol. 21, no. 3, pp. 1167–1179, Mar. 2020.

[4] H. Zhang and J. Wang, "Vehicle lateral dynamics control through AFS/DYC and robust gain-scheduling approach," *IEEE Trans. Veh. Technol.*, vol. 65, no. 1, pp. 489–494, Jan. 2016.

[5] M. S. Mamlouk, "General outlook of pavement and vehicle dynamics," *J. Transp. Eng.*, vol. 123, no. 6, pp. 515–517, Nov. 1997.

[6] G. G. Stokes, "Discussion of a differential equation relating to the breaking of railway bridges," in *Transactions of the Cambridge Philosophical Society*, vol. 8. pp. 707–735.

[7] C. P. Tan and S. Shore, "Response of horizontally curved bridge to moving load," *J. Struct. Division*, vol. 94, no. 9, pp. 2135–2154, Sep. 1968.

[8] E. C. Ting and M. Yener, "Vehicle-structure interactions in bridge dynamics," *Shock Vib. Dig.*, vol. 15, no. 12, pp. 3–9, Dec. 1983.

[9] H. P. Lee, "Dynamic response of a beam with intermediate point constraints subject to a moving load," *J. Sound Vib.*, vol. 171, no. 3, pp. 361–368, Mar. 1994.

[10] Y.-B. Yang, J. Yau, Z. Yao, and Y. Wu, *Vehicle-Bridge Interaction Dynamics: With Applications to High-Speed Railways*. Singapore: World Scientific, 2004.

[11] C. Johansson, C. Pacoste, and R. Karoumi, "Closed-form solution for the mode superposition analysis of the vibration in multi-span beam bridges caused by concentrated moving loads," *Comput. Struct.*, vol. 119, pp. 85–94, Apr. 2013.

[12] S. Sivaraman and M. M. Trivedi, "Looking at vehicles on the road: A survey of vision-based vehicle detection, tracking, and behavior analysis," *IEEE Trans. Intell. Transp. Syst.*, vol. 14, no. 4, pp. 1773–1795, Dec. 2013.

[13] D. M. Bevly, J. Ryu, and J. C. Gerdes, "Integrating INS sensors with GPS measurements for continuous estimation of vehicle sideslip, roll, and tire cornering stiffness," *IEEE Trans. Intell. Transp. Syst.*, vol. 7, no. 4, pp. 483–493, Dec. 2006.

[14] D. Cebon, "Theoretical road damage due to dynamic tyre forces of heavy vehicles part 2: Simulated damage caused by a tandem-axle vehicle," *Proc. Inst. Mech. Eng., C, J. Mech. Eng. Sci.*, vol. 202, no. 2, pp. 109–117, Mar. 1988.

[15] L. Frýba and C. R. Steele, "Vibration of solids and structures under moving loads," *ASME. J. Appl. Mech.*, vol. 43, no. 3, p. 524, 1976.

[16] J. W. Smith, "Vibration of structures: Applications in civil engineering design," *Eng. Struct.*, vol. 11, no. 3, p. 203, 1989.

[17] S. Yim, J. Choi, and K. Yi, "Coordinated control of hybrid 4WD vehicles for enhanced maneuverability and lateral stability," *IEEE Trans. Veh. Technol.*, vol. 61, no. 4, pp. 1946–1950, May 2012.

[18] H. Liang, J. Wu, S. Mumtaz, J. Li, X. Lin, and M. Wen, "MBID: Micro-blockchain-based geographical dynamic intrusion detection for V2X," *IEEE Commun. Mag.*, vol. 57, no. 10, pp. 77–83, Oct. 2019.

[19] B. Ji, Y. Han, P. Li, S. Mumtaz, and H. Wen, "Research on secure transmission performance of electric vehicles under Nakagami-*m* channel," *IEEE Trans. Intell. Transp. Syst.*, vol. 22, no. 3, pp. 1881–1891, Mar. 2021.

[20] N. Deepa *et al.*, "A survey on blockchain for big data: Approaches, opportunities, and future directions," 2020, *arXiv:2009.00858*. [Online]. Available: https://arxiv.org/abs/2009.00858

[21] Y. Sun, J. Xu, G. Lin, W. Ji, and L. Wang, "RBF neural network-based supervisor control for maglev vehicles on an elastic track with network time-delay," *IEEE Trans. Ind. Informat.*, early access, Oct. 19, 2020, doi: 10.1109/TII.2020.3032235.

[22] Y. Sun, J. Xu, H. Wu, G. Lin, and S. Mumtaz, "Deep learning based semi-supervised control for vertical security of maglev vehicle with guaranteed bounded airgap," *IEEE Trans. Intell. Transp. Syst.*, early access, Jan. 1, 2021, doi: 10.1109/TITS.2020.3045319.

[23] D. J. Cole and D. Cebon, "Spatial repeatability of dynamic tyre forces generated by heavy vehicles," *Proc. Inst. Mech. Eng., D, J. Automobile Eng.*, vol. 206, no. 1, pp. 17–27, Jan. 1992.

[24] D. Cebon, "Interaction between heavy vehicles and roads," SAE Tech. Paper 0148-7191, 1993.

[25] A. C. Collop and D. Cebon, "Parametric study of factors affecting flexible-pavement performance," *J. Transp. Eng.*, vol. 121, no. 6, pp. 485–494, Nov. 1995.

[26] D. J. Cole and D. Cebon, "Truck suspension design to minimize road damage," *Proc. Inst. Mech. Eng., D, J. Automobile Eng.*, vol. 210, no. 2, pp. 95–107, Apr. 1996.

[27] T. Potter, D. Cebon, and D. Cole, "Assessing 'road-friendliness': A review," *Proc. Inst. Mech. Eng., D, J. Automobile Eng.*, vol. 211, no. 6, pp. 455–475, 1997.

[28] A. Malekjafarian, P. J. McGetrick, and E. J. OBrien, "A review of indirect bridge monitoring using passing vehicles," *Shock Vib.*, vol. 2015, Mar. 2015, Art. no. 286139.

[29] Y. B. Yang and J. P. Yang, "State-of-the-art review on modal identification and damage detection of bridges by moving test vehicles," *Int. J. Struct. Stability Dyn.*, vol. 18, no. 02, Feb. 2018, Art. no. 1850025.

[30] T. J. Matarazzo and S. N. Pakzad, "Scalable structural modal identification using dynamic sensor network data with STRIDEX," *Comput.-Aided Civil Infrastruct. Eng.*, vol. 33, no. 1, pp. 4–20, Jan. 2018.

[31] Y. Yang and C. Lin, "Vehicle–bridge interaction dynamics and potential applications," *J. Sound Vib.*, vol. 284, pp. 205–226, Jun. 2005.

[32] A. Malekjafarian and E. J. OBrien, "Identification of bridge mode shapes using short time frequency domain decomposition of the responses measured in a passing vehicle," *Eng. Struct.*, vol. 81, pp. 386–397, Dec. 2014.

[33] H. Aied, A. González, and D. Cantero, "Identification of sudden stiffness changes in the acceleration response of a bridge to moving loads using ensemble empirical mode decomposition," *Mech. Syst. Signal Process.*, vols. 66–67, pp. 314–338, Jan. 2016.

[34] X. Q. Zhu, S. S. Law, L. Huang, and S. Y. Zhu, "Damage identification of supporting structures with a moving sensory system," *J. Sound Vib.*, vol. 415, pp. 111–127, Feb. 2018.

[35] S. A. Lippmann, W. A. Piccin, and T. P. Baker, "Enveloping characteristics of truck tires—A laboratory evaluation," in *Proc. Int. Automot. Eng. Congr. Expo.*, 1965, doi: 10.4271/650184.

[36] K. C. Chang, F. B. Wu, and Y. B. Yang, "Disk model for wheels moving over highway bridges with rough surfaces," *J. Sound Vibrat.*, vol. 330, no. 20, pp. 4930–4944, Sep. 2011.

[37] X. Yin, C. S. Cai, Z. Fang, and L. Deng, "Bridge vibration under vehicular loads: Tire patch contact versus point contact," *Int. J. Struct. Stability Dyn.*, vol. 10, no. 3, pp. 529–554, Sep. 2010.

[38] L. Deng, R. Cao, W. Wang, and X. Yin, "A multi-point tire model for studying bridge–vehicle coupled vibration," *Int. J. Struct. Stability Dyn.*, vol. 16, no. 8, 2016, Art. no. 1550047.

[39] Y. Ding, W. Zhang, and F. T. K. Au, "Effect of dynamic impact at modular bridge expansion joints on bridge design," *Eng. Struct.*, vol. 127, pp. 645–662, Nov. 2016.

[40] K. Guo, "Tire roller contact model for simulation of vehicle vibration input," SAE Tech. Paper 0148-7191, 1993.

[41] S. S. Law and X. Q. Zhu, "Bridge dynamic responses due to road surface roughness and braking of vehicle," *J. Sound Vib.*, vol. 282, nos. 3–5, pp. 805–830, Apr. 2005.
[42] J.-C. Wyss, D. Su, and Y. Fujino, "Prediction of vehicle-induced local responses and application to a skewed girder bridge," *Eng. Struct.*, vol. 33, no. 4, pp. 1088–1097, Apr. 2011.
[43] Z. Sun, T. Nagayama, D. Su, and Y. Fujino, "A damage detection algorithm utilizing dynamic displacement of bridge under moving vehicle," *Shock Vib.*, vol. 2016, Jan. 2016, Art. no. 8454567.
[44] S. Neves, A. Azevedo, and R. Calçada, "A direct method for analyzing the vertical vehicle–structure interaction," *Eng. Struct.*, vol. 34, pp. 414–420, Jan. 2012.
[45] S. Neves, P. Montenegro, A. Azevedo, and R. Calçada, "A direct method for analyzing the nonlinear vehicle–structure interaction," *Eng. Struct.*, vol. 69, pp. 83–89, Jun. 2014.
[46] Y. Zhang, H. S. Zhao, and S. T. Lie, "A simple approach for simulating the road surface roughness involved in vehicle-bridge interaction systems," *Int. J. Struct. Stability Dyn.*, vol. 18, no. 07, Jul. 2018, Art. no. 1871009.
[47] D. Y. Zhu, Y. H. Zhang, and H. Ouyang, "A linear complementarity method for dynamic analysis of bridges under moving vehicles considering separation and surface roughness," *Comput. Struct.*, vol. 154, pp. 135–144, Jul. 2015.
[48] Y. Zhang, H. Zhao, and S. T. Lie, "A nonlinear multi-spring tire model for dynamic analysis of vehicle-bridge interaction system considering separation and road roughness," *J. Sound Vib.*, vol. 436, pp. 112–137, Dec. 2018.
[49] S. Wu, H. Ai, Y. Guo, and Q. Fei, "Vibration analysis of a beam on a moving vehicle under the road excitation with different contact models," *J. Vibroeng.*, vol. 15, no. 4, pp. 1689–1700, 2013.
[50] *Mechanical Vibration-Road Surface Profiles-Reporting of Measured Data*, Standard ISO8608, 1995.
[51] K. Liu, E. Reynders, G. De Roeck, and G. Lombaert, "Experimental and numerical analysis of a composite bridge for high-speed trains," *J. Sound Vib.*, vol. 320, nos. 1–2, pp. 201–220, Feb. 2009.
[52] M. Géradin and D. J. Rixen, *Mechanical Vibrations: Theory and Application to Structural Dynamics*. Hoboken, NJ, USA: Wiley, 2014.
[53] *Mechanical Vibration-Road Surface Profiles-Reporting of Measured data*, Standard ISO 8608, 1995.
[54] H. Chen and W. Jin, "Improved pseudo-random excitation method for passive suspension of half vehicle system," *Int. J. Performability Eng.*, vol. 16, pp. 930–940, Jun. 2020.
[55] M. Agostinacchio, D. Ciampa, and S. Olita, "The vibrations induced by surface irregularities in road pavements–a MATLAB approach," *Eur. Transp. Res. Rev.*, vol. 6, no. 3, pp. 267–275, 2014.

Hui Chen received the bachelor's degree in mechanical design, manufacturing, and automation, the master's degree in measurement technology and instrumentation, and the Ph.D. degree in mechanical design and theory from the Lanzhou University of Technology, Lanzhou, China, in 2006, 2012, and 2021, respectively. He is currently with the School of Mechanical and Electrical Engineering, Lanzhou University of Technology. His research interests and directions: nonlinear vibration and control, remote intelligent communication technology, embedded system development, signal processing, and vehicle system dynamics.

Wuyin Jin received the bachelor's degree in engineering in 1992, the master's degree from the Gansu University of Technology in 1997, and the Ph.D. degree from Xi'an Jiaotong University in 2004. From 1997 to 1998, he was with the Akita Prefecture Industrial Technology Center. From 2008 to 2009, he was a Visiting Scholar with the University of Marburg, Germany. He is currently a Professor with the School of Mechanical and Electrical Engineering, Lanzhou University of Technology. His research interests are signal processing, machine learning and image processing, nonlinear dynamics, neuroscience, and dynamics system analysis.

Jiamin Xuan received the Ph.D. degree in mechanical design and theory from China Agricultural University, Beijing, China, in 2015. She is currently a Lecturer with the Zhejiang Institute of Mechanical and Electrical Engineering and holds a joint postdoctoral position with the Lanzhou University of Technology and Zhejiang Changer Intelligent Equipment Company Ltd., China. Her research interests include mechanical design, numerical simulation, and manufacturing engineering.